Biosensors

DOI: 10.1002/anie.201108007

Plasmon Shaping by using Protein Nanoarrays and Molecular Lithography to Engineer Structural Color**

*Alasdair W. Clark and Jonathan M. Cooper**

Localized plasmonic resonances (LSPR) in metallic nanoparticles form the basis for a wide variety of applications based on the concentration and redistribution of light energy.[1,2] LSPR manipulation may occur through geometric and elemental modification of the nanometal, allowing resonant tuning to perform a variety of functions, ranging from the creation of metamaterials with a negative index of refraction to energy harvesting for solar-panel technology.[3,4]

Plasmonics can also be used as a means to monitor nanoscale interactions,[5–7] particularly in biosensors and medical diagnostics, where gold nanoparticles have found a range of applications as chemically stable labels in affinity binding.[8] In such cases, LSPR affects the particle's absorptive and scattering properties, resulting in a readily observable structural color (i.e. color caused by plasmonic effects, not by pigment). The size of the gold nanoparticles (typically < 100 nm) determines the wavelength of resonances they support. This structural color can be used to create colorimetric biosensors; for instance, colloidal aggregation, mediated through the hybridization of nanoparticle-labeled DNA,[9,10] allows the plasmon of discrete particles to interact, shifting the resonance of the system to lower frequencies and changing its color. Related methods have been described using molecular self-assembly of a variety of biomolecules,[10–12] which have relied upon plasmon shifts resulting from random aggregations, either in solution or on surfaces, with little or no control over the number and location of binding events.[13,14] Other techniques which seek to construct nanoparticle networks have relied on binding nanoparticles to surface-based DNA origami.[15–17] To date, such studies have concentrated solely on chemically synthesized nanoparticles, and although there has been great progress in this area in recent years, there remains significant hurdles in the production of high-quality, arbitrary nanoparticle geometries and complex arrayed designs.

Here, we bridge the gap between the versatility of direct-write nanolithography, and the unrivalled resolution and selectivity of molecular self-assembly. We show, for the first time, the molecularly mediated placement, with nm accuracy, of single Au nanoparticles within a pre-fabricated, engineered plasmonic array. In doing so we create coupled plasmonic systems which allow colorimetric, naked-eye detection of protein–protein binding at extreme sensitivities.

By utilizing an engineered approach to molecule-driven plasmon coupling, we precisely create Au heterodimers (the combination of single, lithographically defined nanostructures with single Au nanoparticles) by using site-specific, single molecular binding events. This allows us to optically alter the response of the array, controlling the wavelength of supported surface plasmon modes, and thus the resulting color, in response to individual affinity interactions between proteins. By using protein patterning and alignment techniques at resolutions approaching the length scales of individual antibodies (ca. 5 nm), we ensure only a single binding site is available beside each feature, creating distinctive visual color changes at extreme sensitivities. Not only does this work advance molecular nanoparticle assembly (providing specific, molecularly selective localization of single nanoparticles, which can be applied uniformly over large areas), it also represents a step-change in visible colorimetric biosensing using plasmonics.

Fabrication of the device required two lithography steps followed by several chemical and molecular modification steps. Figures 1 and 2 show diagrammatic illustrations and SEM images, respectively, of these processes. In detail, a plasmonic Au nanoarray was first defined on a glass substrate in poly(methyl methacrylate) (PMMA) resist using electron-beam lithography and electron-beam metal evaporation. Aligned to this Au array was an array of windows, fabricated proximal to the structures in a second PMMA layer, with an accuracy of ca. 5 nm in both the x and y axis (Figures 1a and 2b). Three 500 μm square arrays of gold discs were made with a diameter of 80, 120, and 150 nm, respectively, each with a thickness (z) of 30 nm. The discs were chosen such that the LSPR of each array occurred within the visible spectrum at 563, 595, and 633 nm, respectively.

After the windows were patterned (as a 60 nm square), the glass substrate was functionalized by using well-established aminopropyltriethoxysilane (APTS) and gluteraldehyde immobilization chemistries, enabling attachment of the primary antibody.[18,19] Only those areas of the glass substrate exposed by the windows underwent modification, allowing high-resolution nanopatterning of the capture antibody.

The nanoparticle-modified secondary antibody (goat anti-rabbit immunoglobulin G (IgG) modified with 40 nm Au particles) was then spotted onto the pattern and incubated overnight at 4 °C. The unbound particles were removed by thoroughly rinsing the sample, leaving only those bound specifically to the modified areas (Figures 1c and 2c).

[*] A. W. Clark, J. M. Cooper
Biomedical Engineering Research Division
University of Glasgow, Rankine Building
Oakfield Avenue, Glasgow, G128LT (UK)
E-mail: jon.cooper@glasgow.ac.uk

[**] The authors thank the RASOR interdisciplinary research collaboration initiative, BBSRC, EPSRC and the Scottish Funding Council for funding of this research.

Supporting information for this article is available on the WWW under http://dx.doi.org/10.1002/anie.201108007.

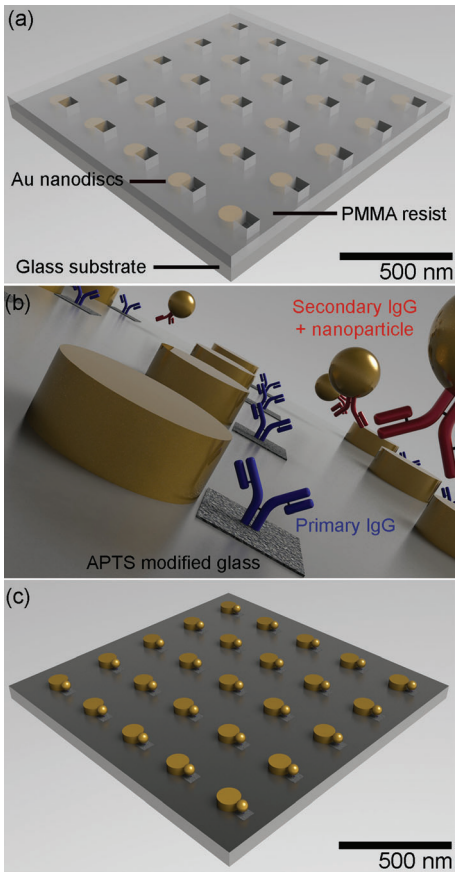

Figure 1. A diagrammatic illustration of the engineered assay (panel (b) is not to scale). a) Windows aligned to the individual array structures are opened up in a resist layer. The area of the glass substrate exposed by these windows was modified with APTS. The resist is stripped, leaving the APTS patterned glass, which is then modified, in turn, with gluteraldehyde and the primary antibody. b) The secondary antibody-conjugated colloid was introduced to the surface. c) After washing, only those areas modified with primary antibody exhibit a nanoparticle bound to the surface.

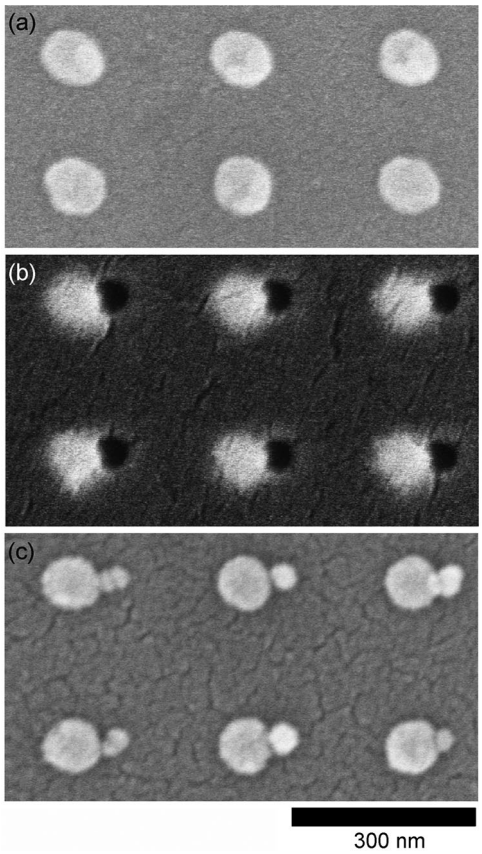

Figure 2. SEM images: a) Array of 120 nm diameter, 30 nm tall gold nanodiscs. b) Windows of 60 nm in dimension, aligned to the original structures and opened up in a secondary layer of resist to allow surface modification of the substrate. c) After antibody binding, showing single, 40 nm diameter gold nanoparticles bound directly adjacent to fabricated features.

The geometry of the engineered plasmonic features, the windows, and the dimensions of the gold nanoparticles were strictly controlled in order to create heterodimers that produce a visible color change in response to single molecule binding events.

The dimensions of the windows were chosen such that the area of surface modification was approximately the size of a single nanoparticle. This helped to promote single binding events across the array (minimizing the chances that more than one particle would occupy the binding zone), allowing us to dictate the number of binding events which took place.

Figures 1c and 2c show the typical colloidal distribution achieved after heterodimer formation. By controlling the position of single metallic particles around the nanodiscs, we alter the structure's LSPR, and thus of the visual response across the whole array. The induced surface charges around each structure are dependent upon their orientation with respect to the driving electromagnetic field. When the incident electric field is polarized across the heterodimeric particle pair axis, the plasmon of the neighboring structures are excited in-phase. In turn, this implies that the surface charges in the region between the two plasmonic entities are opposite, allowing dipole coupling to take place. This has two further results; firstly, the localization of the plasmon in this area leads to an amplification of the electric field; secondly, and most significantly, the resonance frequency of the plasmon (which can be thought of as a fluctuating electron gas, shared by the coupled bodies) is decreased.[20–22]

Figure 3 shows both measured and predicted extinction spectra for each array structure, before and after plasmonic coupling. The experimental resonance wavelengths of the 80, 120, and 150 nm diameter gold discs were 563, 595, and 633 nm, respectively. After binding, as a result of plasmonic coupling to the 40 nm gold particle, a red-shift of 13, 23, and 16 nm, respectively, was measured. In addition to the resonance shift, the plasmon of each array experiences an increase in spectral breadth (a result of an increased plasmon relaxation time).[21,23] The modeled data showed good correlation with experiment, exhibiting a red-shift of 20, 15, and 11 nm for the 80, 120, and 150 nm diameter features, respectively, consistent both with the experimental results shown in Figure 3, and with other current experimental and simulated nanoparticle systems already described in the literature[24–27] (slight colloid inhomogeneity and the resultant

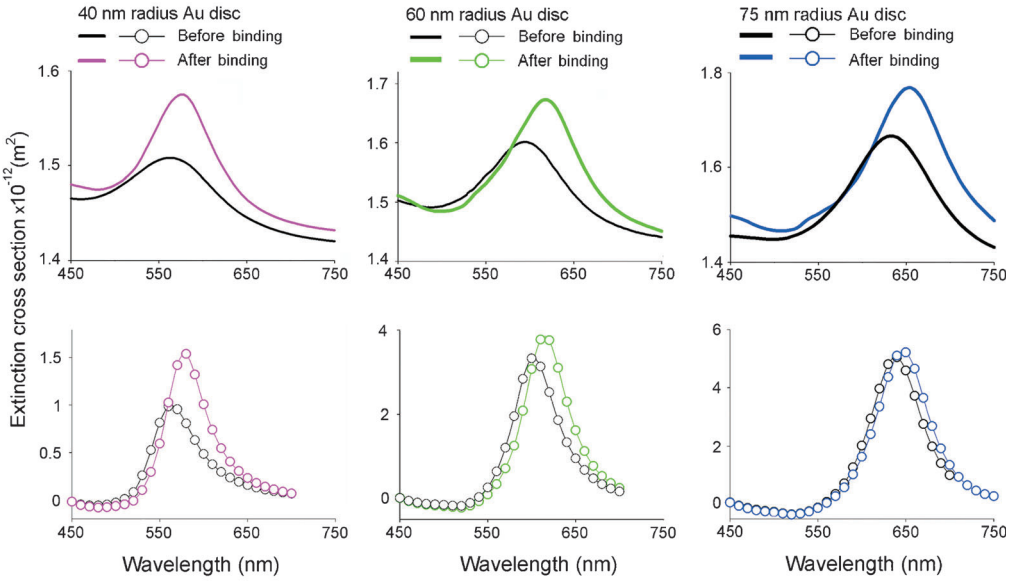

Figure 3. Extinction spectra. Experimental (top) and simulated (bottom) extinction spectra of each array before and after plasmonic coupling.

nm positional shifts from dimer to dimer in the arrayed assay are likely due to the experimental results not perfectly matching simulation).

Figure 4 shows the simulated electric-field distribution around an 80 nm diameter gold disc prior to and after coupling to a 40 nm Au particle. As well as the spectral shift seen in Figure 3, the localized electric field enhancement is significantly increased. The maximum field enhancement experienced by the isolated disc is <100, whereas the coupled system experiences enhancements of >900 in the gap between the nanoparticle and the disc. These results indicate that the technology has the potential to provide an extremely effective surface enhanced Raman sattering (SERS) substrate for the detection and characterization of the molecules located within this region following nanoparticle binding (Raman enhancements of 10^{11} will be experienced by molecules in this area).

The wavelength shifts generated by the 500 μm square sensor arrays are large enough for the color change to be observed by eye. Figure 5 shows a bright-field image of each sensor array before and after heterodimer formation. As stated, this ease of use makes the technology suitable for biosensor applications, with significant advantages over traditional fluorophore or dye-based systems in terms of stability and ease of visualization after protein binding has been completed. The plasmonic effect of gold nanoparticles does not bleach or quench with time, and is not effected by environmental factors such as temperature changes or oxidative effects.

Our technique provides a high degree of structural uniformity, resulting in identical plasmonic field distributions around each feature in the array, making the visual color change homogeneous across large areas. In contrast to those devices which rely on the uncontrolled, randomized binding of many nanoparticles to a functionalized surface particle, this ensures the color change is distinctive enough to be observed by eye, without the need for complex microscopy setups[13,14] (features which make this technology a good fit for point-of-care diagnostic applications).

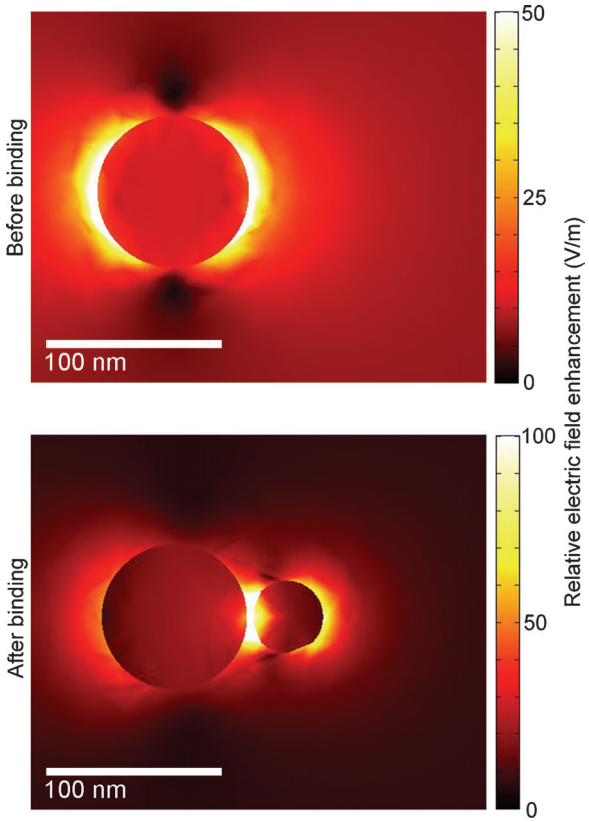

Figure 4. Simulation of plasmonic interaction. Resonant electric-field enhancement of an isolated 80 nm diameter gold nanodisk, and that of one aligned to a 40 nm gold particle, taken as a slice through the *z* axis center of the features. The values of relative electric-field enhancement assume the incident electric field had a value of 1 V m^{-1}. Scales have been chosen to best represent the field distribution and do not represent the maximum field values.

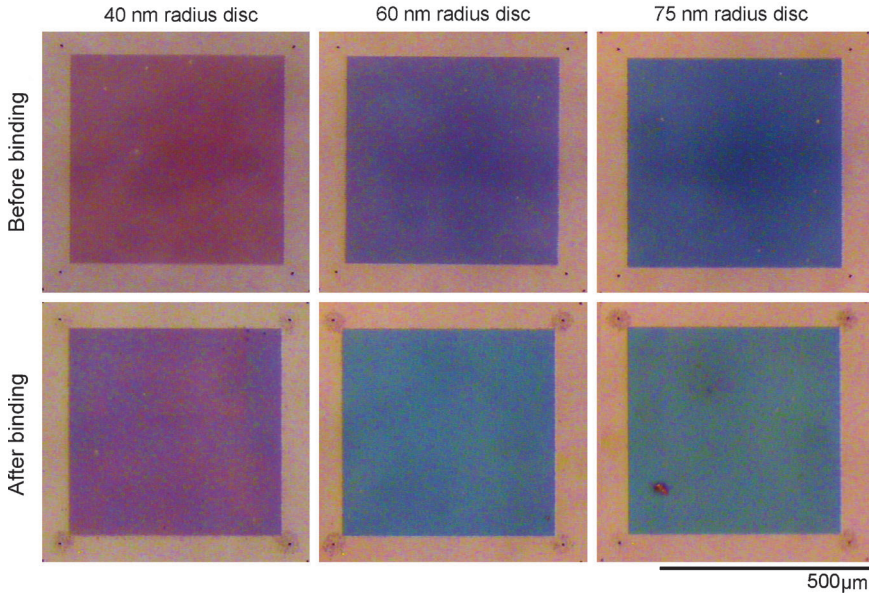

Figure 5. Visual color change. Bright-field images of each sensor array before and after the antibody binding event. Images were taken of each sensor array using a Leica MZ12 microscope, in conjunction with a Ganz ZC-Y11PH3 CCD.

Figure 5 shows arrays of 500 μm in size, although we have observed that color switching can be readily distinguished by eye in sensor as small as 100 μm square, and that color changes in sensors of 10 μm square can easily be observed using a low magnification bright-field microscopes (sizes compatible with lab-on-a-chip). Since each individual binding event is strictly engineered to produce a homogeneous plasmonic response across the array, the visual sensitivity of the technique is extremely high. For example, taking into account the number of binding sites available in the array, Figure 5 illustrates naked-eye observation of protein affinity-binding corresponding to the detection of atto-moles of IgG (equivalent, in our experimental method, to a theoretical limit of pM sensitivity), while the 10 μm sensors allow visualization of approximately 600 individual binding events. Furthermore, because the color shift of the scattered light is identical for each heterodimer, and is not determined by the number of plasmonic elements in the array, this technology is capable of detecting single molecule binding events using the appropriate instrumentation (dark-field microscopy, for instance).

The color shift can be quantified using a jpeg image taken with a standard cell-phone CMOS camera in conjunction with a basic image processing software package (many of which are included on phones themselves). Figure 6 shows bright-field images of the 120 nm diameter disc sensor array, before and after the antibody binding, taken using a 5-megapixel cell-phone camera, along with a RGB color histogram produced using Adobe Photoshop.

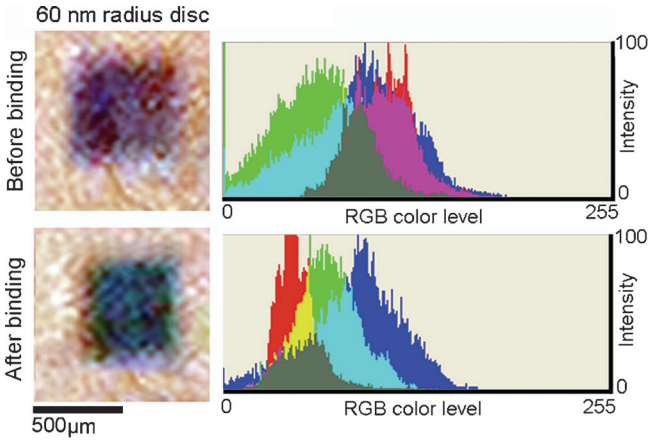

Figure 6. Cell-phone quantification of the sensor. Cell-phone camera image and RGB color histogram 120 nm diameter disc sensor. 8-bit RGB jpeg images taken using a 5 megapixel camera-phone in direct sunlight. Adobe Photoshop was used to analyze the RGB color levels of each array (each channel of an RGB image, red, green, and blue, are assigned a value from 0–255, along with an intensity).

The combination of this sensor technology with cell-phone analysis has clear implications in low-cost, point-of-care diagnosis. For example, in recent years there has been a trend towards cell-phone readable platforms for field diagnostics in the developing world, as they provide a means to easily record and transmit information which can be stored or analyzed off-site. In the future, we foresee these devices being engineered more cost effectively using a combination of soft-lithographic and dip-pen nano-patterning techniques.[28–31] This, combined with a microfluidic delivery device, may facilitate a new generation of high sensitivity tools based upon engineering plasmonic coupling, whilst further increasing their relevance as disposable, point-of-care diagnostic devices.

We have demonstrated the first engineered example of molecularly mediated plasmon shaping in a nanostructured photonic array, where individual structures are tuned by specific translocation of single nanoparticles through antibody affinity-binding. By engineering the geometry, size, and alignment of both the nanophotonic elements and the nanopatterned protein array we control the assembly of heterodimeric plasmonic complexes at single-protein resolutions. Our novel technique enables us to control the extent and nature of the plasmonic coupling, thereby altering the observed structural color. This technology represents a step-change in plasmonic biosensing, offering a visual readout, observable by the naked-eye, to report upon protein binding at sensitivities far exceeding that of other plasmonic, colorimetric methods. In addition, this work provides a new model for molecular nanolithography, where individual binding events can be engineered over large areas, and with protein scale precision, within pre-defined, engineered nanoarrays.

Experimental Section

Primary antibody immobilization: The sample was placed in a 5% APTS solution, in ethanol, for 4 h. The sample was then rinsed with ethanol and placed in an 80°C oven for 1 h. On removal from the oven the resist, which defined the windows was lifted off by soaking in warm acetone for 5 min, leaving the nanopatterned APTS. The sample was then placed in a 2.5% gluteraldehyde solution, in deionized water, for 2 h. After extensive rinsing in deionized water and phosphate-buffered saline (PBS), the primary antibody, rabbit IgG (Sigma–Aldrich), diluted to 10 $\mu g\,mL^{-1}$ in 0.1M carbonate buffer, was spotted (1 μL) onto the modified area and incubated overnight at 4°C. The sample was then rinsed thoroughly, in sequence, with carbonate buffer, PBS + 0.05% Triton X-100, PBS + 1% bovine serum albumine (BSA; to block unbound aldehyde groups), and, finally, with PBS.

Secondary antibody binding: A 3.2 $\mu g\,mL^{-1}$ solution, in 0.1M carbonate buffer, of anti-rabbit IgG, conjugated to 40 nm colloidal gold (BBInternational), was spotted (1 μL) onto the array and incubated overnight at 4°C. The array was then washed thoroughly with PBS + 0.05% Triton X-100, followed by deionized water, to remove any unbound antibody. The antibody-modified colloid had a plasmon resonance, in solution, of 520 nm.

Modeling: COMSOL finite element method (FEM) analysis was used to simulate the plasmonic response of three systems designed to accurately represent the dimensions of those demonstrated experimentally. The extinction cross-section was calculated for each disc before and after antibody-mediated Au nanoparticle binding (the nanoparticle was placed within the simulations at a separation of 3 nm, as measured experimentally by SEM). The electric field of the exciting light was polarized across the particle-pair axis.

Received: November 14, 2011
Published online: January 24, 2012

Keywords: biosensors · colloids · nanomaterials · optical properties · proteins

[1] P. V. Kamat, *J. Phys. Chem. C* **2007**, *111*, 2834.
[2] S. Lal, S. Link, N. J. Halas, *Nat. Photonics* **2007**, *1*, 641.
[3] V. M. Shalaev, *Nat. Photonics* **2007**, *1*, 41.
[4] H. A. Atwater, A. Polman, *Nat. Mater.* **2010**, *9*, 205.
[5] N. L. Rosi, C. A. Mirkin, *Chem. Rev.* **2005**, *105*, 1547.
[6] F. M. Huang, J. J. Baumberg, *Nano Lett.* **2010**, *10*, 1787.
[7] X. Y. Zhang, E. M. Hicks, J. Zhao, G. C. Schatz, R. P. Van Duyne, *Nano Lett.* **2005**, *5*, 1503.
[8] M. C. Daniel, D. Astruc, *Chem. Rev.* **2004**, *104*, 293.
[9] H. X. Li, L. Rothberg, *Proc. Natl. Acad. Sci. USA* **2004**, *101*, 14036.
[10] R. Elghanian, J. J. Storhoff, R. C. Mucic, R. L. Letsinger, C. A. Mirkin, *Science* **1997**, *277*, 1078.
[11] L. R. Hirsch, J. B. Jackson, A. Lee, N. J. Halas, J. West, *Anal. Chem.* **2003**, *75*, 2377.
[12] J. W. Liu, Y. Lu, *Angew. Chem.* **2006**, *118*, 96; *Angew. Chem. Int. Ed.* **2006**, *45*, 90.
[13] W. P. Hall, S. N. Ngatia, R. P. Van Duyne, *J. Phys. Chem. C* **2011**, *115*, 1410.
[14] J. R. Waldeisen, T. Wang, B. M. Ross, L. P. Lee, *ACS Nano* **2011**, *5*, 5383.
[15] C. A. Mirkin, R. L. Letsinger, R. C. Mucic, J. J. Storhoff, *Nature* **1996**, *382*, 607.
[16] S. J. Tan, M. J. Campolongo, D. Luo, W. L. Cheng, *Nat. Nanotechnol.* **2011**, *6*, 268.
[17] J. W. Zheng, P. E. Constantinou, C. Micheel, A. P. Alivisatos, R. A. Kiehl, N. C. Seeman, *Nano Lett.* **2006**, *6*, 1502–1504.
[18] J. N. Lin, J. Herron, J. D. Andrade, M. Brizgys, *IEEE Trans. Biomed. Eng.* **1988**, *35*, 466.
[19] C. R. Suri, M. Raje, G. C. Mishra, *Biosens. Bioelectron.* **1994**, *9*, 535.
[20] C. Bohren, D. Huffman, *Absorption and Scattering of Light by Small Particles*, Wiley, New York, **1983**.
[21] U. Kreibig, M. Vollmer, *Optical Properties of Metal Clusters*, Springer, Berlin, **1995**.
[22] S. A. Maier, *Plasmonics: Fundamentals and Applications*, Springer, New York, **2007**.
[23] M. L. Brongersma, P. G. Kik, *Surface Plasmon Nanophotonics*, Springer, Dordrecht, **2007**.
[24] A. W. Clark, J. M. Cooper, *Adv. Mater.* **2010**, *22*, 4025.
[25] A. W. Clark, J. M. Cooper, *Small* **2011**, *7*, 119.
[26] B. Lamprecht, G. Schider, R. T. Lechner, H. Ditlbacher, J. R. Krenn, A. Leitner, F. R. Aussenegg, *Phys. Rev. Lett.* **2000**, *84*, 4721.
[27] W. Rechberger, A. Hohenau, A. Leitner, J. R. Krenn, B. Lamprecht, F. R. Aussenegg, *Opt. Commun.* **2003**, *220*, 137.
[28] K. L. Kelly, E. Coronado, L. L. Zhao, G. C. Schatz, *J. Phys. Chem. B* **2003**, *107*, 668.
[29] C. L. Haynes, R. P. Van Duyne, *J. Phys. Chem. B* **2001**, *105*, 5599.
[30] R. D. Piner, J. Zhu, F. Xu, S. H. Hong, C. A. Mirkin, *Science* **1999**, *283*, 661.
[31] K. B. Lee, S. J. Park, C. A. Mirkin, J. C. Smith, M. Mrksich, *Science* **2002**, *295*, 1702.

